



Modelling headspace dynamics in modified atmosphere packaged meat

Jon Tofteskov^a, Mari Ann Tørngren^b, Nicholas P. Bailey^a, Jesper Schmidt Hansen^{a,*}

^a IMFUFA, Dept. of Science and Environment, Roskilde University, Universitetsvej 1, P. O. Box 260, 4000, Roskilde, Denmark

^b DMRI, Danish Technological Institute, Gregersensvej 9, 2630, Taastrup, Denmark



ARTICLE INFO

Keywords:

MAP
Mathematical model
Bacterial growth
Oxygen consumption
Carbon dioxide dissolution

ABSTRACT

The dynamics of bacterial growth and concentrations of oxygen and carbon dioxide in the headspace of modified atmosphere packaged (MAP) meat is studied. The work is based on extensive long-time storage experiments on pork chops lasting up to 42 days at temperatures 0 °C and 5 °C and four different headspace gas mixtures with 10%, 20%, 40% and 70% oxygen and 30% carbon dioxide. The headspace dynamics is modelled. The model includes oxygen consuming biochemical processes in the meat and also the coupling between headspace and meat, specifically, the diffusion of oxygen and carbon dioxide into the meat. The model is parametrized from the experimental data, and captures the experimental results. It is concluded that the oxygen consuming processes inside the meat packed with MAP consume less than 1% of the initial oxygen in the headspace, and are not important for the headspace dynamics. On the other hand, the dissolution of carbon dioxide has a significant effect. This is due to the relatively large solubility of carbon dioxide compared to oxygen. From the model we find and characterize three distinct phases behind the headspace volume reduction observed. As the model is dynamical and mechanistic it can be used to give information about the retail-packed fresh meat under different oxygen containing atmospheres, effects of leaks, and more.

1. Introduction

A long shelf life requires maintaining quality parameters such as color, odour, and texture at optimum as well as keeping it safe to eat for as long as possible (Subramaniam and Wareing, 2016). Improved predictive accuracy of the shelf life will help minimize waste (Wikström et al., 2014; Quedsted et al., 2013) by reducing the incidence of discarding food which has reached its labeled shelf life, but is still both appealing and safe to eat. Many factors affect shelf life, through many mechanisms, making accurate prediction of shelf life challenging. The first step towards more accurate shelf life labelling is understanding the most important mechanisms that cause food quality and safety to degrade, and how they interact with each other.

Mathematical modelling will play an increasing role (Riva et al., 2009; Chaix et al., 2014, 2015; Belay et al., 2016) in improving shelf life, both in understanding the basic shelf-life determining processes, and in developing tools to estimate the shelf life for different conditions. We can start to gain better understanding by modelling the physical, chemical and biological processes that play a role for the shelf life of meat. Here physical processes include the transport of water, oxygen, carbon dioxide and nitrogen by diffusion in and out of the food product (Zaritzky and Bevilacqua, 1988); chemical processes include

oxidation of lipids, proteins, and mitochondrial respiration (Tang et al., 2005), and biological processes are the growth of spoilage and pathogenic bacteria (Van Boekel, 2008; Jay et al., 2005; Aberle et al., 2012). A large literature of modelling such processes in food exists, see for example Zaritzky and Bevilacqua (1988); Saenz et al. (2008), although to our knowledge no work has involved including all three kinds of process in the same model.

In the case of fresh meat typical packing techniques are Modified Atmosphere Packaging (MAP) (McMillin, 2008; Singh et al., 2011). With MAP the gas composition of the headspace environment is modified, typically, by having large partial pressures of oxygen and carbon dioxide compared to ambient conditions. In contrast to other foods such as fruits and vegetables, where a low oxygen concentration is typically required, oxygen concentrations in MA packaged meat can vary from zero up to 70–80% in order to preserve the red color of the meat by binding to myoglobin (Antonini and Brunori, 1971).

Previous work (Tofteskov et al., 2017) described the transport of oxygen in meat and its reactions with myoglobin. The boundary condition was a fixed concentration of oxygen at the surface of the meat. Thus, there was in effect an unlimited supply of oxygen. In the present work we model the headspace dynamics, giving a more realistic meat-headspace boundary condition for common storage conditions. The

* Corresponding author.

E-mail address: jshmidt@ruc.dk (J.S. Hansen).

model includes bacterial growth, the associated oxygen consumption, and carbon dioxide production in the headspace. Furthermore, headspace gasses penetrate the meat surface, and are dissolved and consumed by various biochemical processes. We also include these processes in the model in order to investigate the importance of these. The model involves several parameters, and we extract these from the experimental data for pork. It is important to point out that the model is general can be applied to other meat types by reparametrization.

2. Materials and Methods

The experimental part of this work was a meat storage experiment lasting 42 days where fresh pork chops were stored at two different temperatures and under four different gas environments. On the day of slaughter, 45 pig carcasses were selected according to gender (female) and carcass weight (79–87 kg). The day after slaughter, pH was measured in the left loin (5.5–5.6) and both left and right sides of 30 carcasses were selected. Thereafter, the carcasses were cut and de-boned into loins. The loins were crust frozen in an impingement freezer and then sliced into 150 g chops with an approximate thickness of 1.75 cm and volume $244 \pm 5 \text{ cm}^3$. Chops with common cutting surface were packed pairwise in boxes and then transported at 0°C to the Danish Meat Research Institute (DMRI) packaging pilot facility, where the meat was prepared and packaged on that same day. The temperature during transport was measured with two Testo T174 temperature loggers.

Packing and storage: Each pair were then MA-packed in a tray with specifications K2190–53H MAPET II (Færsh Plast, Holstebro Denmark). The film was a $45 \mu\text{m}$ anti-fogging film TOPLEX HB B-PE 45 F (Plastopil, Almere, Netherlands) using a tray sealer Multivac, T200, Denmark. The water vapour transmission rate (WVTR) for this film is 10 g m^{-2} per day at 90% relative humidity and 38°C , and the transmission rate for oxygen at 23°C is $4 \text{ cm}^3 \text{ m}^{-2}$ per day (Plastopil, 2014). The total tray volume was 900 cm^3 resulting in a headspace volume to meat volume ratio of approximately 2.7. All four gas compositions were mixed onsite with a PBI-mixer and contained 30% carbon dioxide (lying in the interval used by the industry) and nitrogen (filler gas). To study the system dynamics and model performance under different oxygen conditions the initial oxygen levels were set to 10%, 20%, 40% and 70%. The samples were then stored in darkness for up to 23 days at 5°C and for up to 42 days at 0°C . For each storage temperature samples were collected 9 times during the storage period.

At each sampling day, where the day index indicates the day after slaughter, the pork chops were analyzed for psychrotrophic bacteria ($6.5^\circ\text{C}/10$ days, PCA). When sampling for the psychrotrophic plate count, 10 cm^2 of the lean meat surface was marked, removed and transferred to a stomacher bag. To each bag, 100 mL of buffered peptone water was added, and the bag was stomached for 1 min. The samples were then diluted, plated on PCA and incubated at 6.5°C for 10 days (NMKL No. 86, 5th Ed., 2013).

Oxygen and carbon dioxide gas compositions were measured using a Checkmate 3, PBI Dansensor, Denmark with tolerance of $\pm 2\%$. Once a sample is taken the entire package was discarded. This then leads to a total of 480 samples covering the four gas mixtures and two temperatures.

3. Mathematical model

A schematic presentation of the system is shown in Fig. 1. We model a section of the meat-surface system. The gas is assumed to be well mixed which means that there are no gradients present in the headspace. This assumption is reasonable since the diffusive processes in the gas phase happen on a fast time scale compared to the time scales of interest in the meat. For example, in the meat the diffusion coefficient for oxygen is in the order of $10^{-5} \text{ cm}^2 \text{ h}^{-1}$ (Chaix et al., 2014), whereas in air it is $18 \text{ cm}^2 \text{ h}^{-1}$ at 0°C (Lide, 1976), that is, for a package height of 5 cm the time for diffusion to equalize the concentration is around 1 h.

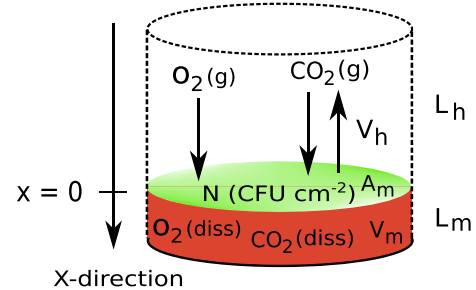


Figure 1. [Color online] Schematic illustration of the system. The gas (top) with volume $V_h = 0.66 \text{ L}$ is assumed to be a homogeneous mixture of carbon dioxide, oxygen and inert filler gas. The meat structure is homogeneous, but we do not assume a homogeneous distribution of the dissolved oxygen in the meat. The meat has volume $V_m = 0.24 \text{ L}$. On top of the meat is a thin layer of bacteria with area $A_m = 163 \text{ cm}^2$ that consumes the oxygen from the packaging and produce carbon dioxide on formation. L_h and L_m denote the headspace and meat heights, respectively, such that $V_h = A_m L_h$ and $V_m = A_m L_m$. N is the number of bacteria per unit square centimeter, estimated experimentally in terms of colony-forming units (CFU). The values for volumes and area are taken from the experimental setup.

Nitrogen gas is an inert gas and it is assumed to have no effect on the meat bio-chemistry. However, nitrogen will dissolve in the meat leading to a reduced head-space volume. It is possible to estimate this reduction using the solubility of nitrogen in water which is $0.03 \text{ g per kg water at } 0^\circ\text{C and } 1 \text{ atm}$ (Lide, 1976). The meat volume is 0.24 L , hence, the volume of the dissolved nitrogen is around $5 \times 10^{-3} \text{ L}$, which is less than 0.8% of the total headspace volume. Since this reduction is relatively small compared to the reduction due to carbon dioxide absorption we do not include the nitrogen gas dynamics in the model. The film used in the experiment has a very low permeability with respect to both oxygen and water vapour (see Materials and Methods section), hence, we expect a very low permeability for carbon dioxide as well, and the gas flow out of the package can be considered to be zero.

Bacteria are primarily concentrated on the surface of the meat (Selgas et al., 1993) although a small anaerobic microbiological activity is also present inside the meat (Aberle et al., 2012). Therefore, the bacterial growth rate depends primarily on the concentration of available oxygen and carbon dioxide in the headspace, and the growth process consumes oxygen and produces carbon dioxide (Chaix et al., 2014). The meat structure is assumed to be homogeneous on the small cuts we study, that is, we do not consider the effects of fat, bones and so forth. Finally, the model does not include effects of the changing pH-values inside the meat and on the meat surface.

In the model we include oxygen and carbon dioxide dissolution and consumption in the meat. Thus, the dynamics is given by five dynamical variables, namely, the number of bacteria per unit area, and the amount of oxygen and carbon dioxide in both the headspace and the meat. We will make an approximation (see later) such that the oxygen in the meat can be expressed by the headspace oxygen, i.e., the final model has four dynamical variables.

3.1. Bacterial growth and headspace dynamics

The experiments were performed under oxygen-rich conditions at temperatures 0°C and 5°C , and we therefore assume that the main bacterial growth is due to psychrophilic aerobic bacteria growth on the meat surface (Aberle et al., 2012). This also includes microaerophilic bacteria that can grow in reduced oxygen concentrations (Molin, 2000). In the following N denotes the number of bacteria per unit area on the meat surface. Bacterial growth is typically prefaced by a lag phase with virtually no growth. An exponential like growth then occurs up to a carrying capacity, N_{max} . As the bacterial concentration N approaches N_{max} the growth rate slows down and the population enters a stationary,

Table 1

Top section: Best fit parameter values from data. Middle section: Estimated parameter values. Bottom section: Literature values from Chaix et al. [Chaix et al. \(2015\)](#).

		0 °C	5 °C
C_{ox}	[M]	8.9×10^{-3}	10.1×10^{-3}
μ_{opt}	[h ⁻¹]	1.4×10^{-2}	3.6×10^{-2}
k_{resp}	[mol cm ^{-2(1-\alpha)} CFU ^{-\alpha}]	3.7×10^{-9}	2.8×10^{-9}
$N(0)$	[CFU cm ⁻²]	77	128
<hr/>			
k_2	[L h ⁻¹]	0.05	0.5
$\sqrt{k_{conD}}$	[cm h ⁻¹]	0.01	
α		0.5	
N_{max}	[CFU cm ⁻²]	10^7	
<hr/>			
S_{CO_2}	[M atm ⁻¹]	3×10^{-2}	2×10^{-2}
$CO_{2,max}$	[M]	0.11	
S_{O_2}	[M atm ⁻¹]	1.4×10^{-4}	

or saturation, phase. The growth stage is modelled by what are known as primary models ([Chaix et al., 2015](#)). Primary models are sufficient to model the bacterial growth if the surrounding conditions are constant, i.e., if the system is defined by constant oxygen concentration, pH values, etc. Secondary models are needed to include these changing environmental conditions ([Chaix et al., 2015](#)). As our primary bacterial growth model, we use the simple logistic differential equation ([Zwietering et al., 1990](#)), however, note that this model does not explicitly model the lag time. The differential logistic equation reads

$$\frac{dN}{dt} = \mu_{max} N \left(1 - \frac{N}{N_{max}} \right). \quad (1)$$

μ_{max} is the maximum rate of change and depends on the oxygen and carbon dioxide concentrations ([Chaix et al., 2015](#); [Baez and Shiloach, 2014](#); [Ercolini et al., 2006](#)) and is given by the secondary models. The model parameters and their units are listed in [Table 1](#) and [Fig. 1](#).

To include the dependence of carbon dioxide and oxygen we need a secondary model and we choose the standard γ -factor approach ([Chaix et al., 2014](#)). First, the rate of change, dN/dt , increases as a function of the oxygen for low oxygen concentrations, but will decrease when the oxygen levels are very high as oxygen then acts as an inhibitor for growth ([Höll et al., 2016](#); [Molin, 2000](#)). Carbon dioxide we treat as an inhibitor ([Geysen et al., 2006](#)) such that the maximum rate of change decreases monotonically for increasing concentrations of carbon dioxide. μ_{max} can then be written as a product of these two mechanisms

$$\mu_{max} = \mu_{opt} \gamma_{O_2} \gamma_{CO_2}, \quad (2)$$

where μ_{opt} is a coefficient independent of the oxygen and carbon dioxide concentrations. We express the oxygen dependence, γ_{O_2} , by the functional form

$$\gamma_{O_2} = \frac{4[O_2]C_{ox}}{(C_{ox} + [O_2])^2}. \quad (3)$$

Note, this function is unity when $[O_2] = C_{ox}$, the optimal value, and goes to zero at both lower and higher oxygen concentrations. In this way we have included the possible inhibitory effect of oxygen at large oxygen concentrations.

The inhibition, γ_{CO_2} , is simply linear with respect to carbon dioxide, see for example [Geysen et al. \(2006\)](#):

$$\gamma_{CO_2} = 1 - \frac{[CO_2]}{CO_{2,max}}, \quad (4)$$

where $CO_{2,max}$ is a model parameter.

Next we model the total amount of oxygen, n_{O_2} , and carbon dioxide, n_{CO_2} , in headspace. To this end, we need an expression for the bacterial respiration rate. This has not been studied very extensively according to [Chaix et al. \(2015\)](#), but work by [Riedel et al. \(2013\)](#) indicates that oxygen consumption rate per bacterium is much greater in the growth phase than in the stationary phase ([Chaix et al., 2015](#); [Garcia-Ochoa et al., 2010](#)). This is confirmed for oxygen levels 10–40% in our experiments. To show this we define the relative oxygen consumption as $\Delta n_{O_2} = 1 - n_{O_2}(t)/n_{O_2}(0)$ which can be found directly from the experimental data. [Fig. 2 \(a\)](#) shows the rate of headspace oxygen consumption per bacterium versus the bacterial concentration N for oxygen levels 10–40%. Note that both axes are logarithmic. It is clearly observed that for small bacterial concentrations (growth regime) the consumption rate per bacterium is large compared to when the bacterial concentration is close to the bearing capacity. At the 70% O_2 level the data are very noisy and this conclusion cannot be confirmed for this particular case.

From [Fig. 2 \(b\)](#) it is further seen that the oxygen consumption is not proportional with the bacterial concentration, and therefore dn_{O_2}/dt is not proportional to dN/dt . This we attribute to the bacteria adaption to the changing environment (the bacteria become less aerobic) ([Höll et al., 2016](#)), and not due to processes in the meat. Since dn_{O_2}/dt is not proportional to dN/dt , we can in general let dn_{O_2}/dt be proportional to $f(N) dN/dt$. The data in [Fig. 2 \(b\)](#) suggest that f follows a power law with respect to N , where the exponent is $\alpha - 1$ with $0 < \alpha < 1$. From [Eq. \(1\)](#) we then have

$$\frac{dn_{O_2}}{dt} = -k_{resp} A_m \mu_{max} N^\alpha \left(1 - \frac{N}{N_{max}} \right) - r_{O_2}, \quad (5)$$

where k_{resp} is the proportionality constant, A_m is the surface area (see [Fig. 1](#)) and r_{O_2} describes the rate of change due to processes in the meat; we address the latter below.

Respiration is characterized by a one-to-one relationship between the bacterial consumption of oxygen and the production of carbon dioxide ([Andersen and von Meyenburg, 1980](#)), i.e., in the headspace we have $dn_{CO_2} = -dn_{O_2}$. This gives us the following dynamics for the headspace carbon dioxide

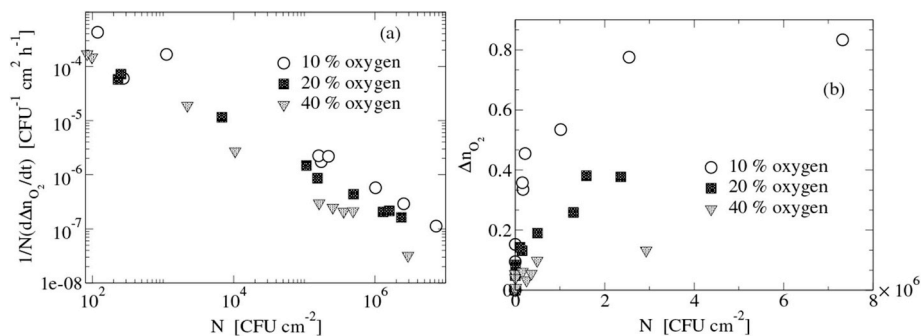


Fig. 2. (a) Relative oxygen consumption rate per bacterium versus bacterial concentration. The oxygen consumption is defined as $\Delta n_{O_2} = 1 - n_{O_2}(t)/n_{O_2}(0)$. (b) Headspace oxygen consumption versus bacterial concentration. In both (a) and (b) the temperature is 0 °C, and the data shown are averages over five samples.

$$\frac{dn_{CO_2}}{dt} = k_{resp} A_m \mu_{max} N^\alpha \left(1 - \frac{N}{N_{max}}\right) - r_{CO_2}, \quad (6)$$

where r_{CO_2} is the drain due to carbon dioxide solubility in meat.

3.2. Dynamics in the meat

Equations (1), (5) and (6) are the dynamical equations for the headspace dynamics. The two terms r_{O_2} and r_{CO_2} account for the coupling to processes in the meat. Oxygen will diffuse into the meat and chemical processes like oxidation of fats, vitamins and myoglobin take place. Mitochondrial respiration is another important oxygen consuming process (Tofteskov et al., 2017). To simplify the problem we let the chemical oxygen consumption in the meat be linearly dependent on the concentration of oxygen, and we therefore have the following reaction-diffusion equation for the oxygen concentration in the meat

$$\frac{\partial [O_2]}{\partial t} = -k_{con} [O_2] + D \frac{\partial^2 [O_2]}{\partial x^2}, \quad (7)$$

where D is the diffusion coefficient of oxygen in meat and k_{con} is the rate constant governing the chemical consumption in the meat. Recently, we have shown (Tofteskov et al., 2017) that the oxygen profile reaches a steady-state on a time scale of hours at 20 °C. While temperatures here are lower we assume that the quasi steady-state condition $[\dot{O}_2] = 0$ is reached on time scales smaller than those we study here. Then Eq. (7) reduces to an ordinary differential equation

$$\frac{d^2 [O_2]}{dx^2} - \frac{k_m}{D} [O_2] = 0, \quad (8)$$

with boundary conditions $[O_2](0)$ at $x = 0$ and $[O_2](L_m) = 0$ at $x = L_m$, where L_m is the meat depth, see Fig. (1). The later condition is met if the meat thickness is sufficiently large such that $e^{-\sqrt{k_{con}/D} L_m} \simeq 0$. This boundary value problem has the solution

$$[O_2](x) = [O_2](0) e^{-\sqrt{k_{con}/D} x} = S_{O_2} RT \frac{n_{O_2}}{V_h} e^{-\sqrt{k_{con}/D} x}, \quad (9)$$

where S_{O_2} is the solubility of oxygen in meat, and R the gas constant. From this concentration profile we can evaluate the total oxygen consumption in the meat by integration and by noting that the consumption is linear with respect to the oxygen concentration

$$r_{O_2} = k_{con} A_m \int_0^{L_m} [O_2](x) dx = S_{O_2} RT \frac{\sqrt{k_{con} D}}{L_h} n_{O_2}. \quad (10)$$

Note that by introducing the quasi steady-state condition we can avoid including the dynamics of the oxygen in meat explicitly.

Finally, we address the issue of carbon dioxide in the meat. First, we will ignore any possible chemical reaction with carbon dioxide in the meat, and also assume that the carbon dioxide produced in the mitochondrial respiration is negligible compared to the amount of carbon dioxide coming from diffusion. Therefore, the governing process behind the carbon dioxide dynamics in the meat is simple diffusion. The diffusion coefficient for carbon dioxide, D_{CO_2} , is independent of the type of product and found to be in the range 1–543 mm²h⁻¹ (Chaix et al., 2014). Using median value for the diffusion coefficient the characteristic penetration depth, $\ell = \sqrt{2D_{CO_2} t}$, is then around 10 cm after 24 h. Thus, after one day ℓ is one order of magnitude larger than the meat depth $L_m \approx 1.8$ cm, and we assume that there are no relevant carbon dioxide gradients in the meat on the time scales we investigate here. Of course, on smaller time scales the carbon dioxide dynamics should be modelled using the diffusion equation. Furthermore, we let the carbon dioxide be fully dissolved, thus, the equilibrium concentration of carbon dioxide in the meat is given by $[CO_2] = S_{CO_2} p_{CO_2}$, where S_{CO_2} is the solubility coefficient and $p_{CO_2} = n_{CO_2} RT/V_h$ the partial pressure of CO₂ in the headspace. In the linear regime we can then write the carbon dioxide drain as

$$r_{CO_2} = k_2 \left(\frac{S_{CO_2} RT n_{CO_2}}{V_h} - \frac{n_{CO_2}^m}{V_m} \right), \quad (11)$$

where k_2 is the rate constant and $n_{CO_2}^m$ is the amount of carbon dioxide in the meat volume V_m . This linear kinetics does not properly account for diffusion, but it does account correctly for the equilibrium solubility and assigns a reasonable time scale to the absorption, which is sufficient to match the available data.

Substituting Eqs. (11) and (10) into Eqs. (5) and (6) we arrive at the final model

$$\frac{dN}{dt} = \mu_{max} N \left(1 - \frac{N}{N_{max}}\right) \quad (12)$$

$$\frac{dn_{O_2}}{dt} = -k_{resp} A_m \mu_{max} N^\alpha \left(1 - \frac{N}{N_{max}}\right) - S_{O_2} RT \frac{\sqrt{k_{con} D}}{L_h} n_{O_2} \quad (13)$$

$$\frac{dn_{CO_2}}{dt} = k_{resp} A_m \mu_{max} N^\alpha \left(1 - \frac{N}{N_{max}}\right) - k_2 \left(\frac{S_{CO_2} RT n_{CO_2}}{V_h} - \frac{n_{CO_2}^m}{V_m} \right) \quad (14)$$

$$\frac{dn_{CO_2}^m}{dt} = k_2 \left(\frac{S_{CO_2} RT n_{CO_2}}{V_h} - \frac{n_{CO_2}^m}{V_m} \right), \quad (15)$$

where $\mu_{max} = \mu_{max}(n_{O_2}, n_{CO_2})$ can be written in terms of the total amount of oxygen and carbon dioxide in the headspace rather than concentrations

$$\mu_{max}(n_{O_2}, n_{CO_2}) = \mu_{opt} \left(\frac{4n_{O_2} C_{ox}}{V_h C_{ox}^2 + n_{O_2}^2/V_h + 2C_{ox} n_{O_2}} \right) \left(1 - \frac{n_{CO_2}}{V_h CO_{2,max}}\right). \quad (16)$$

A short comment is in order here. First, there are two competing processes consuming oxygen, namely, bacterial growth and the mitochondrial respiration in the meat. Due to the latter we have $n_{O_2} \rightarrow 0$ as $t \rightarrow \infty$. Thus, mitochondria in the meat can consume, given sufficient time, arbitrarily large amounts of oxygen, which is not the case in reality, hence, the model is only valid up to intermediate times. To our knowledge, no detailed data of the post mortem mitochondrial lifetime is available, so we cannot model the changing mitochondria activity in greater detail.

4. Parameter estimation

From literature values (Chaix et al., 2015) we can find the solubilities S_{O_2} and S_{CO_2} , and $CO_{2,max}$. The parameters $\sqrt{k_{con} D}$, α , N_{max} , and k_2 are estimated from Fig. 2 and raw data. N_{max} is set to 10⁷ CFU cm⁻² in agreement with data and we have noticed that $\sqrt{k_{con} D}$ has to be sufficiently small (less than 0.02 cm h⁻¹) to keep the observed anti-correlation between the oxygen and carbon dioxide time series. From Fig. 2 we set $\alpha = 1/2$, and k_2 is set such that the CO₂ time series approximately agrees with the first experimental data point, see Fig. 4 and Table 1. Our model is then a function of parameters, $\theta = (C_{ox}, \mu_{opt}, k_{resp}, N(0))$, time, t , and initial conditions $n_{O_2}(0)$, $n_{CO_2}(0)$ and $n_{CO_2}^m(0)$. Note, that we treat the initial bacterial concentration as a fitting parameter. Also, note that the experiment provides data for the bacterial concentration as well as oxygen and carbon dioxide concentrations in headspace, but not for the carbon dioxide dissolved in the meat, and we can only use the former three quantities for the fitting procedure.

For each temperature and sampling times $t_1, t_2, \dots, t_i, \dots$ we have five samples for the three quantities. The sample means of these are denoted $\mu_{\log_{10} N}(t)$, $\mu_{n_{O_2}}(t)$, and $\mu_{n_{CO_2}}(t)$ and the standard deviation $\sigma_{\log_{10} N}(t)$, $\sigma_{n_{O_2}}(t)$ and $\sigma_{n_{CO_2}}(t)$. Importantly, for the bacterial concentration we use the logarithm when determining the contributions to the cost function. In order to estimate the best fit parameters of the model, i.e., to determine the best parameter set θ , we then define the standard cost-function

$$C(\theta) = \sum_n \sum_i \left[\frac{\left(\mu_{\log_{10}N}(g_n, t_i) - \log_{10}N(g_n, t_i, \theta) \right)^2}{\sigma_{\log_{10}N}^2(g_n, t_i)} + \frac{(\mu_{O_2}(g_n, t_i) - n_{O_2}(g_n, t_i, \theta))^2}{\sigma_{O_2}^2(g_n, t_i)} + \frac{(\mu_{CO_2}(g_n, t_i) - n_{CO_2}(g_n, t_i, \theta))^2}{\sigma_{CO_2}^2(g_n, t_i)} \right] \quad (17)$$

where $N(g, t, \theta)$, $n_{O_2}(g, t, \theta)$ and $n_{CO_2}(g, t, \theta)$ are model output for specified initial conditions and parameters θ at time t . The variable g_n is a label for the particular mixtures, i.e., the cost function includes all the available data at a given temperature. Note that fitting is done separately for each temperature. Using appropriate initial parameter values and the Nelder-Mead simplex algorithm (Nelder and Mead, 1965; Eaton et al., 2015) we find a local minimum for the cost function. The cost function for this first estimated set of parameters is denoted $C_0 = C(\theta_0)$.

While a “best-fit” set of parameters can be found by minimizing the cost function, these are of limited use by themselves. One problem which frequently arises is the presence of sloppiness in the parameters, meaning that a parameter, or a particular combination of parameters, can be varied significantly while changing the cost function negligibly. It is important to have a quantitative measure for the accuracy of the parameters, and even more so, for the accuracy of the model output. To investigate the statistical uncertainties we apply the Metropolis Monte-Carlo algorithm. Here the parameters θ iteratively vary in parameter space through $\theta_{new} = \theta_{old} + \delta\theta$, where $\delta\theta$ is a vector with components of small uniformly distributed random numbers with zero mean; this is explained further below. The cost function, C_{new} , is then evaluated with these new parameters, which are always accepted if the cost function is smaller than the current one, C_{old} . Otherwise the new parameter set is accepted if

$$R < \exp \left[-\frac{C_{new} - C_{old}}{T_s} \right] \quad (18)$$

where R is a random number picked from a uniform distribution between 0 and 1, and T_s is here called the sampling temperature as it is analogous to temperature in statistical physics (Frederiksen et al., 2004). A natural choice of T_s is the minimum (best-fit) value C_0 of the cost function scaled by half the number of parameters (Frederiksen et al., 2004), i.e. $T_s = C_0/2$. We only sample in the positive parameter subspace, and the variance of $\delta\theta$ is set such that the acceptance ratio is approximately one half.

By using the Metropolis Monte Carlo algorithm iteratively, we generate an ensemble of 2×10^4 parameter sets which effectively samples the parameter space around the best fit, taking the full non-linearity of the cost function into account. From this ensemble we can evaluate both a model output ensemble mean and variance, which allows for well defined estimates of the model prediction uncertainties. In Fig. 3 (a) we plot, as an example, the histogram for C_{ox} at $T = 0^\circ\text{C}$. It is interesting to see that the distribution is not simply Gaussian, and that the ensemble sample mean does not equal the mode (or most probable value) in the distribution.

For both temperatures, $T = 0^\circ\text{C}$ and 5°C the Metropolis Monte Carlo method did find another cost function minimum, albeit with approximately the same parameter values. In Table 1 we list the best-fit parameters, the parameters estimated from data, and the parameters obtained from the literature (Chaix et al., 2015).

5. Results and discussion

In Fig. 4 experimental non-averaged raw data (filled symbols) are plotted together with model results (lines) for both temperature $T = 5^\circ\text{C}$ (a)-(d) and $T = 0^\circ\text{C}$ (e) and (f). Model results are shown using best fit

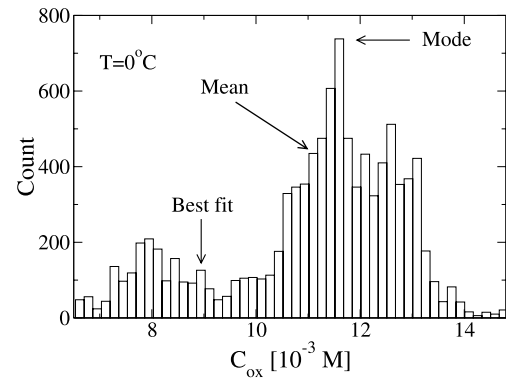


Fig. 3. Parameter ensemble histogram for C_{ox} at $T = 0^\circ\text{C}$. The best fit, mean and mode (most probable) values are indicated.

parameters (black lines), and model output ensemble mean (brown lines). First, we see that the model captures the experimental results quite well, both for varying gas mixtures and varying temperatures. The choice of best fit parameter or ensemble mean values does not significantly change the model output. Secondly, the effect from the carbon dioxide dissolution is clearly observed in the headspace; this is a fast process, and the meat is saturated within approximately 24 h in accordance with our assumption above. Thirdly, the oxygen decrease is strongly correlated with the carbon dioxide increase, that is, the bacterial respiration. This indicates that the oxygen dynamics is governed by the bacterial activity and that the consumption in the meat is very small.

We have also indicated the model output standard deviation for the gases, see dashed lines in Fig. 4 (b), (d), and (f). At the end of the data sampling the uncertainty is around 5 percentage points for all gas compositions. The model output for the bacterial concentration is very skewed and, as is the case for the experimental data, associated with large statistical uncertainties. This is highlighted in Fig. 4 (a) where both the model output median and mean are shown. To give an estimate of the statistical uncertainty the first quartile, Q_1 , and third quartile, Q_3 , are also plotted. For clarity the median and quartiles are omitted in Fig. 4 (c) and (e).

To quantify the oxygen consumption in the meat further, we write the total consumed oxygen in the meat as (see Eq. (10))

$$\Delta n_{O_2}^m(t) = S_{O_2} RT \frac{\sqrt{k_{con} D}}{L_h} \int_0^t n_{O_2}(t') dt'. \quad (19)$$

According to the model, for all headspace mixtures and temperatures the consumed oxygen in the meat at the end of the experiment is less than 1% of initial oxygen in headspace. In fact, the consumption is so low that we can at best estimate an upper limit for this drain through the relevant parameters, namely, $\sqrt{k_{con} D} < 0.02 \text{ cm h}^{-1}$ as mentioned above. In contrast to this approximately 15% of the initial carbon dioxide in headspace will be dissolved in the meat; this depends of course on the meat to headspace ratio and the initial partial pressure.

From the model the total headspace gas reduction can be investigated as a function of storage time; this is plotted in Fig. 5 for the system in Fig. 4(a) and (b). Three distinct phases in the headspace gas reduction are observed. In the first equilibration phase, the carbon dioxide dissolves in the meat reducing the total amount of gas in the headspace. This process is fast and takes place over the first 24 h. The second phase is where the total amount of gas only varies very little; the number of bacteria is relatively small and, as discussed above, the oxygen consumed in the meat is negligible. In this phase the bacteria grows exponentially, but their number is too small to affect the headspace gas. This phase we denote the static phase, albeit it is only approximately static. In the final third phase the bacteria oxygen consumption and therefore carbon dioxide production is at maximum. As

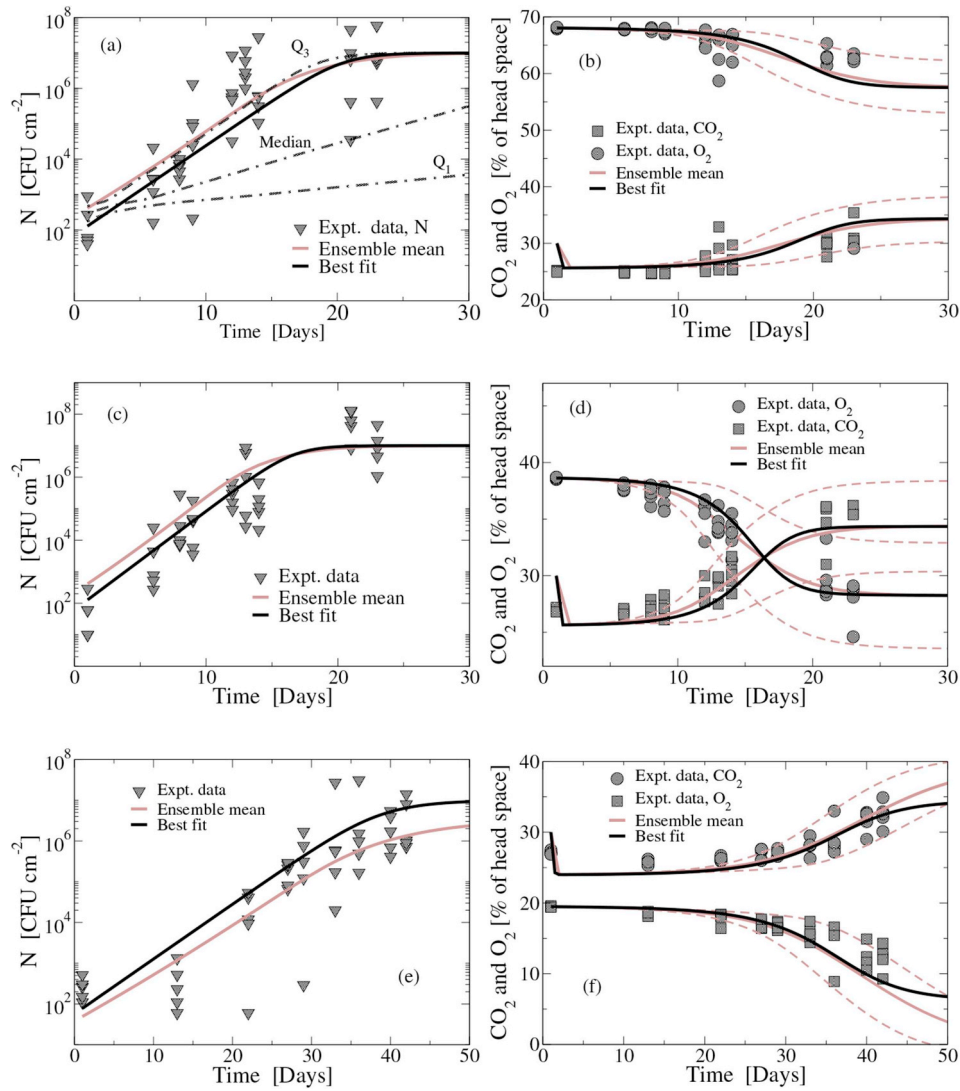


Figure 4. [Color online] Experimental data (filled symbols) and model results (lines). Black lines are model predictions using best fit parameter values and brown lines are model predictions using model output ensemble average. Dotted lines represent the model output standard deviation. (a) and (b): $T = 5\text{ }^{\circ}\text{C}$ and 70% oxygen. (c) and (d): $T = 5\text{ }^{\circ}\text{C}$ and 40% oxygen. (e)–(f): $T = 0\text{ }^{\circ}\text{C}$ and 20% oxygen.

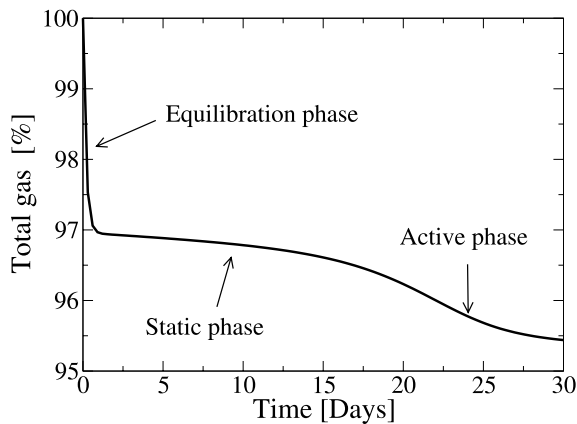


Fig. 5. The total amount of gas in the headspace versus time for $T = 5\text{ }^{\circ}\text{C}$ and 70% oxygen.

the ratio between carbon dioxide and oxygen in headspace increases more gas is dissolved in the meat simply due to the higher solubility of carbon dioxide leading to a reduction in headspace gas. This phase is called the active phase to emphasize the high biological activity. Thus,

the reduced headspace gas phenomenon (package collapse) we attribute to (i) initial dissolution of carbon dioxide and (ii) the relatively high solubility of carbon dioxide compared to oxygen. (Jakobsen and Bertelsen, 2004, 2006). It is worth noting that the three phases are observed for both temperatures and different headspace mixtures. Also, as the total amount of gas is known the package volume can be estimated from the ideal gas law.

If the coupling between headspace and meat is ignored altogether the model reduces to a two dimensional problem, where the dynamical variables are N and n_{O_2} or n_{CO_2} . In this case the oxygen drainage stops when $N = N_{\text{max}}$, in contrast to Eq. (13). Also, here the total amount of headspace gas is conserved and the three headspace gas reduction phases are not present. Fig. 5 gives an indication of the resulting error, compared to Eqs. (12)–(15), from ignoring the coupling; here the total headspace gas reduction is approximately 4.5%, but it can be up to around 10%.

6. Conclusion

In this paper we have proposed a mathematical model for the headspace dynamics of MAP meat. Specifically, the model includes the dynamics of the surface bacterial growth, the headspace oxygen and

carbon dioxide concentrations as well as the carbon dioxide dissolved in the meat. The model was applied to MA packaged pork and parameters were extracted from a series of long-term storage experiments.

From the model we conclude that the oxygen consumption in the meat, i.e., oxidation processes and post mortem mitochondrial respiration, do not affect the headspace dynamics. The carbon dioxide dissolution in the meat, on the other hand, has a significant effect. The headspace gas reduction undergoes three phases: (i) a fast equilibration phase where the carbon dioxide dissolves in the meat, (ii) a static phase where the dynamics is very slow, and (iii) a biologically active phase wherein the bacteria consume large amount of oxygen and produce an equal amount of carbon dioxide, which is then dissolved in the meat. This latter phase is accompanied by a headspace reduction since the carbon dioxide has a relatively large solubility compared to the oxygen. This effect will be stronger for higher initial oxygen concentrations.

Mathematical modelling always involves simplifications and assumptions. For example, in the present model the reaction between carbon dioxide and the water in the meat is not included. This reaction will change the pH-value inside the meat and on the meat surface which in turn inhibits the bacteria growth and the mitochondrial activity (Chaix et al., 2015). It will be interesting to study the pH dynamics in more detail, and include this into an extension of the model. Other extensions of the model include package permeability, which can be modelled by a simple additional term in Eqs. (5) and (6) (but which is not relevant here), anaerobic bacterial dynamics, etc. Apart from extending the model, additional experimental data verifying that the bacterial oxygen consumption rate is decreasing with respect to bacteria count for 70% oxygen levels is needed. Finally, determination of the model parameters for different animals and cuts will make the model applicable for a larger range of different types of meats.

Acknowledgments

This study was supported by a grant for the PRIS Innovation Consortium from The Danish Council for Technology and Innovation [no. 09052174], by the Danish PWT Foundation- Investment in Public Welfare Technology (ABT-fonden), by the Norma & Frode Jacobsens foundation [no. 253] and the Danish Meat Research Institute.

References

- Aberle, E.D., Forrest, J.C., Gerrard, D.E., Edward, W.M., 2012. Principles of Meat Science. W. H. Freeman.
- Andersen, K., von Meyenburg, K., 1980. Are growth rates of *Escherichia coli* in batch cultures limited by respiration? *J. Bacteriol.* 144, 114–123.
- Antonini, E., Brunori, M., 1971. Hemoglobin and Myoglobin in Their Reactions with Ligands. North-Holland.
- Baez, A., Shiloach, J., 2014. Effect of elevated oxygen concentration on bacteria, yeasts, and cells propagated for production of biological compounds. *Microb. Cell Factories* 13. <https://doi.org/10.1186/s12934-014-0181-5>.
- Belay, Z.A., Caleb, O.J., Opara, U.L., 2016. Modelling approaches for designing and evaluating the performance of modified atmosphere packaging (MAP) systems for fresh produce: a review. *Food Pack. Shelf Life* 10, 1–15.
- Chaix, E., Couvert, O., Guillaume, C., Gontard, N., Guillard, V., 2015. Predictive microbiology coupled with gas O₂/CO₂ transfer in food/packaging systems: how to develop an efficient decision support tool for food packaging dimensioning. *Compr. Rev. Food Sci. Food Saf.* 14, 1–21. <https://doi.org/10.1111/1541-4337.12117>.
- Chaix, E., Guillaume, C., Guillard, V., 2014. Oxygen and carbon dioxide solubility and diffusivity in solid food matrices: a review of past and current knowledge. *Compr. Rev. Food Sci. Food Saf.* 13, 261–286. <https://doi.org/10.1111/1541-4337.12058>.
- Eaton, J.W., Bateman, D., Hauberg, S., Wehbring, R., 2015. GNU Octave version 4.0.0 manual: a high-level interactive language for numerical computations. <http://www.gnu.org/software/octave/doc/interpreter>.
- Ercolini, D., Russo, F., Torrieri, E., Masi, P., Villani, F., 2006. Changes in the spoilage-related microbiota of beef during refrigerated storage under different packaging conditions. *Appl. Environ. Microbiol.* 72, 4663–4671. <https://doi.org/10.1128/AEM.00468-06>.
- Frederiksen, S.L., Jacobsen, K.W., Brown, K.S., Sethna, J.P., 2004. Bayesian ensemble approach to error estimation of interatomic potentials. *Phys. Rev. Lett.* 93, 165501. <https://doi.org/10.1103/PhysRevLett.93.165501>.
- García-Ochoa, F., Gomez, E., Santos, V., Merchuk, J., 2010. Oxygen uptake rate in microbial processes: an overview. *Biochem. Eng. J.* 79, 289–307. <https://doi.org/10.1016/j.bej.2010.01.011>.
- Geysen, S., Escalona, V.H., Verlinden, B.E., Aertsen, A., Geeraerd, A.H., Michiels, C.W., Van Impe, J.F., Nicolai, B.M., 2006. Validation of predictive growth models describing superatmospheric oxygen effects on *Pseudomonas fluorescens* and *Listeria innocua* on fresh-cut lettuce. *Int. J. Food Microbiol.* 111, 48–58. <https://doi.org/10.1016/j.jfoodmicro.2006.04.044>.
- Höll, L., Behr, J., Vogel, R.F., 2016. Identification and growth dynamics of meat spoilage microorganisms in modified atmosphere packaged poultry meat by MALDI-TOF MS. *Food Microbiol.* 60, 84–91. <https://doi.org/10.1016/j.fm.2016.07.003>.
- Jakobsen, M., Bertelsen, G., 2004. Predicting the amount of carbon dioxide absorbed in meat. *Meat Sci.* 68, 603–610. <https://doi.org/10.1016/j.meatsci.2004.05.012>.
- Jakobsen, M., Bertelsen, G., 2006. Solubility of carbon dioxide in fat and muscle tissue. *J. Muscle Foods* 17, 9–19. <https://doi.org/10.1111/j.1745-4573.2006.00029.x>.
- Jay, J.M., Loessner, M.J., A., G.D., 2005. *Modern Food Microbiology*. Springer.
- Lide, D.R. (Ed.), 1976. *CRC Handbook of Chemistry and Physics*. CRC Press, Cleveland.
- McMillin, K.W., 2008. Where is MAP Going? A review and future potential of modified atmosphere packaging for meat. *Meat Sci.* 80, 43–65. <https://doi.org/10.1016/j.meatsci.2008.05.028>.
- Molin, G., 2000. Modified atmospheres. In: In: Lund, B., Baird-Parker, T.C., Gould, G.W. (Eds.), *The Microbial Safety and Quality of Food*, vol. 1. Aspen Publishers, Inc, pp. 214–234.
- Nelder, J., Mead, R., 1965. A simplex method for function minimization. *Comput. J.* 7, 308–313.
- Plastopil, N., 2014. Toplex 4b B-pe 45 Af. Datasheet.
- Questaed, T.E., Marsh, E., Stunell, D., Parry, A.D., 2013. Spaghetti soup: the complex world of food waste behaviours. *Resour. Conserv. Recycl.* 79, 43–51. <https://doi.org/10.1016/j.resconrec.2013.04.011>.
- Riedel, T., Berelson, W., Neelson, K., Finkel, S., 2013. Oxygen consumption rates of bacteria under nutrient-limited conditions. *Appl. Environ. Microbiol.* 79, 4921–4931.
- Riva, M., Sinelli, N., Franzetti, L., Torri, L., Limbo, S., 2009. Predictive modeling of the freshness of minced beef meat stored in MAP at different temperatures. *Ital. J. Food Sci.* 21, 14–18.
- Saenz, C., Hernandez, B., Alberdi, C., Alfonso, S., Dineiro, J., 2008. A multispectral imaging technique to determine concentration profiles of myoglobin derivatives during meat oxygenation. *Eur. Food Res. Technol.* 227, 1329–1338. <https://doi.org/10.1007/s00217-008-0848-4>.
- Selgas, D., Marin, M., Pin, C., Casa, C., 1993. Attachment of bacteria to meat surfaces - a review. *Meat Sci.* 34, 265–273. [https://doi.org/10.1016/0309-1740\(93\)90076-T](https://doi.org/10.1016/0309-1740(93)90076-T).
- Singh, P., Wani, A.A., Saengerlaub, S., Langowski, H.C., 2011. Understanding critical factors for the quality and shelf-life of MAP fresh meat: a review. *Crit. Rev. Food Sci.* 51, 146–177. <https://doi.org/10.1080/10408390903531384>.
- Subramanian, P., Wareing, P. (Eds.), 2016. *The Stability and Shelf Life of Food*, second ed. Woodhead.
- Tang, J., Faustman, C., Hoagland, T., Mancini, R., Seyfert, M., Hunt, M., 2005. Postmortem oxygen consumption by mitochondria and its effects on myoglobin form and stability. *J. Agric. Food Chem.* 53. <https://doi.org/10.1021/jf048646o>.
- Tofteskov, J., Hansen, J.S., Bailey, N.P., 2017. Modelling the autooxidation of myoglobin in fresh meat under modified atmosphere conditions. *J. Food Eng.* 214, 129–136. <https://doi.org/10.1016/j.jfoodeng.2017.06.002>.
- Van Boekel, M.A.J.S., 2008. Kinetic modeling of food quality: a critical review. *Compr. Rev. Food Sci. Food Saf.* 7, 144–158.
- Wikström, F., Williams, H., Verghese, K., Clune, S., 2014. The influence of packaging attributes on consumer behaviour in food-packaging LCA studies: a neglected topic. *J. Clean. Prod.* 73, 100–108. <https://doi.org/10.1016/j.jclepro.2013.10.042>.
- Zaritzky, N., Bevilacqua, A., 1988. Oxygen diffusion in meat tissues. *Int. J. Heat Mass Tran.* 31, 923–930. [https://doi.org/10.1016/0017-9310\(88\)90081-6](https://doi.org/10.1016/0017-9310(88)90081-6).
- Zwietering, M.H., Jongenburger, I., Rombouts, F., van 't Riet, K., 1990. Modeling of the bacterial growth curve. *Appl. Environ. Microbiol.* 56, 1875–1881.